Band-gap-related energies of threading dislocations and quantum wells in group-III nitride films as derived from electron energy loss spectroscopy

A. Gutiérrez-Sosa, U. Bangert, and A. J. Harvey
Physics Department, UMIST, Manchester M60 1QD, United Kingdom

C. J. Fall and R. Jones
School of Physics, University of Exeter, Exeter EX4 4QL, United Kingdom

P. R. Briddon
Department of Physics, University of Newcastle upon Tyne, Newcastle NE1 7RU, United Kingdom

M. I. Heggie
CPES, University of Sussex, Falmer, Brighton BN1 9QJ, United Kingdom

(Received 10 October 2001; revised manuscript received 15 April 2002; published 26 June 2002)

We present results of highly localized electron energy loss spectroscopy carried out using scanning transmission electron microscopy in the energy loss regime at band gap and at the nitrogen near-edge structure of cross-sectional GaN, InGaN, and Al(Ga)N structures. We specifically attempt to determine changes in the intensity distribution and the onset energy of the inelastic scattering (the band-gap-related energy), of heterointerfaces, of quantum wells and of dislocations. We have used *ab initio* calculations within the local-density approximation to density-functional theory of the GaN and AlN band structure to simulate low electron energy loss spectra. Tests in which these were compared to experimental low loss spectra of pure GaN and AlN show good agreement in the position and shape of the spectral features. We then compare the positions of the onset energies on traversing interfaces of single AlN and AlGaN quantum wells as well as of GaInN and GaAlN multiple quantum well structures to the pure GaN and AlN spectra. We have been able to map relative changes in band-gap related energies of isolated interfaces and quantum wells, while the energy loss near edge structure allowed us to monitor relative changes in multiple layered structures of less than 5-nm separation. Reasons for the different sensitivities towards the above features, when measured in different energy regimes, are discussed. Following on from this we study the scattering intensity around onset and the position of the onset energy in locations along projection lines of isolated dislocations. Low loss spectrum calculations of dislocated regions reveal band-gap states associated with all dislocation types in GaN. The related pre-band-gap scattering intensity at 3.3 eV of the simulated spectra, in particular for the full core screw dislocation is in qualitative agreement with the experimental findings. An absorption peak at 2.4 eV found in certain regions in the vicinity of dislocations was not reproduced in the calculations and therefore was thought not to be produced by the dislocation but by impurity segregation.

DOI: 10.1103/PhysRevB.66.035302 PACS number(s): 79.20.Uv, 71.55.Gs, 61.72.Ff, 61.43.Bn

I. INTRODUCTION

Most group-III nitride films grown today have high densities of threading dislocations.[1] The electrical activity associated with dislocations has been the focus of a large body of work in recent years.[2–4] The influence of dislocations on the performance of nitride electronic devices is smaller than expected, for reasons that are still not fully understood. Previous work suggested that dislocations in InGaN are screened off due to In depletion around the dislocation, thus isolating it from free carriers.[5] It was also pointed out that phase segregation in InGaN leads to the localization of carriers, which then would not reach the dislocation. However, indium is expected to accumulate at N sites of reduced coordination found in pits that form at the surface of threading dislocations.[6]

Experimental techniques suitable for investigating the electrical activity of dislocations in the nitrides are scant. Atomic force microscopy in combination with photoluminescence studies has shown that threading dislocations, in particular, screw dislocations, can act as nonradiative recombination centers and degrade the luminescence efficiency in the blue part of the spectrum.[7] Cathodoluminescence studies have also shown that the yellow luminescence, which is ascribed to V_{Ga}-O complexes, is spatially nonuniform and can be correlated with extended defects, in particular low-angle grain boundaries.[8]

Spatially resolved electron energy loss spectroscopy (EELS) is a sensitive tool ideally suited for directly probing the electronic structure of dislocations. Misfit dislocations at a GaAs/GaInAs interface have previously been investigated in this way, showing the existence of localized states at the dislocation core.[9] More recently, nitrogen *K*-edge energy-loss near-edge structure (ELNES) measurements have been performed on edge dislocations in GaN, highlighting differences from bulk regions.[10] A similar study in cubic GaN showed mid-gap levels associated with stacking faults near a GaN/GaAs interface.[11]

A number of theoretical investigations of dislocations in GaN have also been carried out. Elsner *et al.*[12] predicted that screw dislocations with closed cores possess midgap states, but open core screw and threading edge dislocations possess

levels closer to the band edges. The authors suggested however, that impurities might accumulate in the vicinity of the dislocation due to the strain field, creating shallow gap states. For edge dislocations, Wright and Grossner found empty levels in the upper half of the gap about 1 eV, from the conduction-band edge.[13] Vacancy accumulation at dislocation cores has also been predicted to generate deep gap states.[13] Under Ga-rich conditions, Ga-filled screw dislocations, which have electronic states throughout the gap, have been predicted to dominate over open-core dislocations.[14]

Using a cold field emission scanning transmission electron microscope (STEM), we have improved the procedure to undertake highly spatially resolved electron energy loss spectroscopy in the extreme low loss regime (lowEELS). In our setup, energies in the range of the GaN band gap are entirely separated from the zero loss peak, thus allowing details of the joint density of states (JDOS)—weighted by wave-function matrix elements—to be obtained without further data processing. Previous experiments required a deconvolution of the zero loss peak, which introduces artifacts and spurious peaks in the lowEELS spectrum. In this paper we study the effect of interfaces, quantum wells, and individual dislocations on the near band edge JDOS of several nitride systems. The lowEELS studies are complemented with information obtained from ELNES and energy dispersive x-ray (EDX) measurements and are compared to theoretical results for EELS spectra. Our studies are performed on Ga(Al)N$[11\bar{2}0]$ cross sections, where the probe can be stepped along dislocation core projections. This allows us to pick up trends in the behavior of the dislocation JDOS. In contrast to results from single measurements, this method increases the confidence level of the conclusions.

In Sec. II, we present the experimental instruments and parameters used, and explain how the full width at half-maximum (FWHM) of the lowEELS zero loss peak can be minimized. Results of theoretical lowEELS calculations are presented in Sec. III, and are compared to experiment. Section IV discusses issues of spatial resolution in a cross-sectional geometry, while Sec. V presents the results obtained for a variety of heterostructures. Finally, the conclusions are detailed in Sec. VI.

II. EXPERIMENTAL SETUP

Three samples are used in this experiment: sample 1, a ~1.5–2-μm-thick *n*-type wurtzite GaN [0001] layer grown by metal organic chemical vapor deposition (MOCVD) on a [0001] sapphire substrate,[15] and containing an InGaN multiple-quantum-well (MQW) array near the surface. Sample 2 consists of GaN layers including AlN and AlGaN single quantum wells (QW's) as well as an AlGaN MQW array near the film surface, grown on a [0001] 6H-SiC substrate. This sample was grown by molecular beam epitaxy.[16] Sample 3 consists of two 1-μm GaN layers on sapphire: the bottom layer, on the sapphire substrate side, is *n* type doped, while the upper layer is *p* type doped. *P* doping with Mg has in the past proven difficult and ineffective. From Hall measurement results on similar material[17] it is disputable whether the *p* dopants in the present sample are actually electrically active. We ought to be able to detect the effects of *p* doping since EEL spectra of dislocations in *n*-doped material should be different from those of *p*-doped material. This sample was grown by MOCVD.

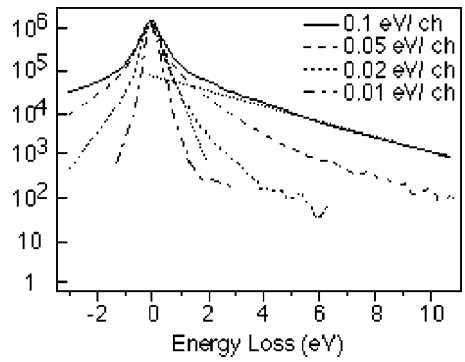

FIG. 1. Logarithmic representation of experimental zero loss peaks obtained with a fresh tungsten tip in a cold FEG and a conventional photodiode array with energy dispersions of 0.1 (solid line), 0.05 (dashed line), 0.02 (dotted line), and 0.01 (dash-dot) eV/channel. The dotted straight lines show the contributions of the FN distribution, and the detector PSF to the zero loss peak.

Imaging in bright field and high angle dark field modes are carried out in a VG601 cold field emission STEM, equipped with EDX and a Parallel Gatan 666 EEL spectrometer at an operating voltage of 100 kV and a probe size of typically 1 nm. The collector aperture angles for lowEELS and ELNES are 3.4 and 6.8 mrad, and the objective aperture angles 5.9 and 10.6 mrad, respectively. LowEELS point spectra are taken with the electron beam stepped across interfaces, across regions where arrays of QW's have been grown, and along individual dislocation lines throughout the film, as well as in the perfect material, for reference.

The energy resolution is dictated by the shape of the zero loss peak (ZLP), arising from a convolution of the Fowler-Nordheim (FN) energy spread function of the gun with the high voltage instability function, which has a Gaussian distribution, and with the spectrometer point spread function (PSF). The FN energy spread function depends on the gun extraction voltage, which should be as small as possible to keep the FWHM at a minimum, but still provide enough counts for acceptable statistics (over 1000 counts/channel in the interband scattering regime). The high voltage instability superimposes a low frequency wobble on the spectra, which, when taken with large acquisition times, creates an increase in the FWHM of the ZLP. This can be counteracted by reducing the acquisition time, but again, care has to be taken to keep the signal to noise ratio in the loss region of interest acceptable. The PSF does not significantly affect the FWHM of the zero loss peak, although it contributes to the extension of its tails.

The crucial factor that influences the energy range of the tail of ZLP is the energy dispersion of the spectrometer (range of energy associated to each photodiode). Figure 1 shows experimental ZLP's obtained using energy dispersion values of 0.1, 0.05, 0.02, and 0.01 eV per channel. The extrapolated straight lines highlight the fact that at energy losses lower than 2 eV it is the FN distribution that affects

the detectability of spectral features. At higher-energy losses, around 3 eV, the FN tail becomes insignificant compared to the tail of the flatter spectrometer PSF. Figure 1 also shows that decreasing the dispersion value (i.e., to 0.01 eV/channel) compresses the FN distribution into a narrower energy regime, so that the PSF tail now is the dominant factor down to 2 eV. The PEELS spectrometer comprises an YAG (yttrium-aluminum-garnet) scintillator coupled via fiber optics to an array of around 1000 semiconductor photodiodes. The long tail of the PSF originates predominantly from scattering processes in the YAG, resulting in the deviation of a large fraction of the light at zero loss into 50 photodiodes on either side of the ZLP. Acquiring spectra with small dispersion values (i.e., a large energy dispersion) moves the spectral features out of this region and therefore reduces the overlap with the PSF tail. From Fig. 1 it becomes obvious that the dispersion of 0.01 eV/channel not only reduces the intensity of the PSF tail at 3 eV by two orders of magnitude compared to the dispersion of 0.1 eV/channel, but also reduces the FWHM of the zero loss peak. The low loss spectra presented in this work are taken with 0.01 eV/channel. The number of spectra, the acquisition time per spectrum and the gun extraction voltage are chosen such that, in combination, they give a FWHM of the zero loss peak of 0.34–0.36 eV, and a statistical error of less than 2% in the loss peak of interest. Acquisition times of individual spectra of up to 1 s could be used without deterioration of the FWHM of the zero loss peak, and the number of spectra taken at each point oscillated between 20 and 50, in order to achieve good statistics without damaging the sample.

Although improvements through deconvolution of the FN spread function (or a pure experimental ZLP) from the low loss spectra have been reported,[18] we found, in agreement with many authors (see, e.g., Ref. 19) that such procedures are notorious for introducing artifacts, especially in the lowEELS region. The ZLP of spectra obtained in our experimental conditions are entirely separated from the structure of the interband scattering region, thus allowing us to dispense with deconvolution techniques. The only data processing undertaken here is the calculation of the first derivative of the raw data, and in some cases, removal of a double exponential background. The latter is fitted to the tail of the zero loss peak in an energy range below the band gap; at the lower end of this energy range the fit deviates rapidly from the ZLP, and hence the low energy limit for our loss signal extraction is usually around 2 eV.

Figure 2 shows raw GaN and AlN low EELS spectra and their first derivatives. The first clear maximum of the EELS derivative is related to the onset of the joint density of states in each material, and is defined here as the EELS onset energy. In the perfect material, i.e., without midgap or near-edge states, it is representative of the position of the conduction band. In material containing defects, such as dislocations, empty gap states might induce a shift of the onset of the low loss signal. The FWHM of our zero loss peak is of the order of 0.34–0.36 eV, and thus our resolving power will be of the order of ± 0.18 eV. For this reason we will not resolve near edge states, e.g., at dislocations as separate peaks, but as a shift in the EELS onset energy. The

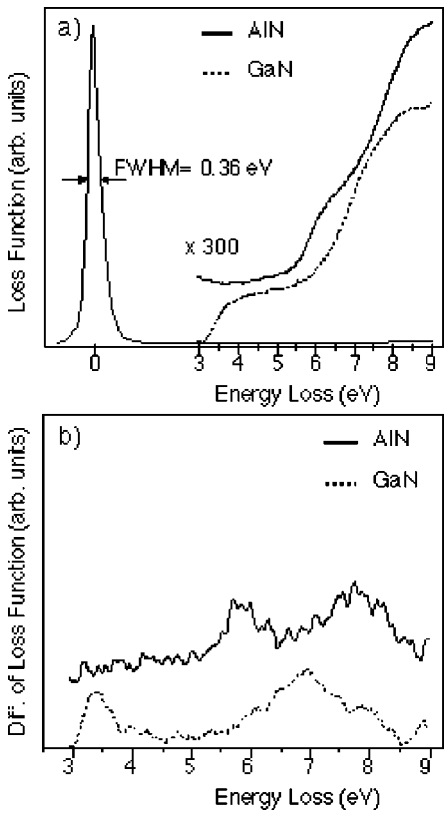

FIG. 2. (a) Raw low electron energy loss spectra (displayed with the zero loss peak as a thin line) of AlN (solid line) and GaN (dashed line), taken with a dispersion value of 0.01 eV/channel. (b) First energy derivative of the raw data.

signal of the surrounding matrix adds to the dislocation signal, making its relative contribution small (see Sec. IV).

ELNES of the N *K* edge are obtained with a dispersion of 0.1 eV per channel at selected points on and off dislocations, as well as inside QW's and barriers separating the QW's. This technique allows significant stoichiometric abnormalities that may be caused by interdiffusion, to be revealed. For comparison x-ray line scans are taken across and along the Al_2O_3/GaN interface in sample 1 and across the SiC/AlN, AlN/GaN, and the GaN/AlGaN interfaces in sample 2.

III. THEORETICAL CALCULATIONS OF ENERGY-LOSS SPECTRA

We perform self-consistent *ab initio* simulations of GaN and AlN within the local density approximation (LDA) to density-functional theory, using the AIMPRO code.[20] The wave functions are expanded in a set of *s*, *p*, and *d* atom-centered Gaussian orbitals. We use pseudopotentials[21] to describe the ion cores and include the nonlinear core correction to account for the Ga $3d$ electrons.

Low loss EELS results from electronic transitions between the valence bands and conduction bands. The signal obtained experimentally is usually interpreted as being representative of $-\mathrm{Im}\{\varepsilon(E)^{-1}\}$, where ε is the dielectric function and E is the energy loss.[22] We calculate the imaginary part of the dielectric function in the dipole approximation for

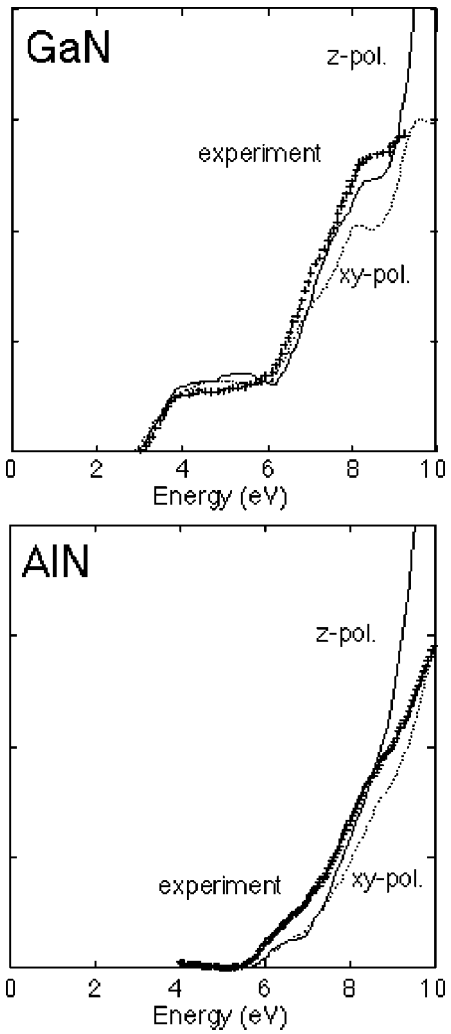

FIG. 3. Comparison between experimental (crosses) and theoretical (lines) low-loss EEL spectra of bulk wurtzite GaN and AlN. The theoretical curves are given for *xy* (dotted line) and *z* (solid line) polarizations of the electric field and are in arbitrary units.

x-, *y*-, and *z*-oriented electric fields.[23] The LDA band gap is adjusted to the experimental value by means of a shift of the conduction bands. The real part of the dielectric function is obtained through a Kramers-Kronig transformation.

The low-loss EELS calculated spectra of bulk GaN and AlN are in Fig. 3, where we compare them with the experimental curves of Fig. 2(a). In view of the cross-sectional acquisition geometry, the experimental low loss spectra correspond to the calculated *xy* polarized results. Qualitative agreement between the computed and measured spectra is obtained, and in particular, the positions of the shoulders in the spectra are well described.

To study dislocations in GaN, an edge-type dislocation dipole is placed within a neutral 144-atom supercell, thus allowing structural periodicity to be retained, and the atoms are relaxed to their equilibrium positions. The band structure associated with an edge dislocation in GaN is shown in Fig. 4(a) along the [0001] core direction. Two states localized on the dislocation core, empty in *p*-doped and undoped material, are found in the top half of the gap. They are expected to

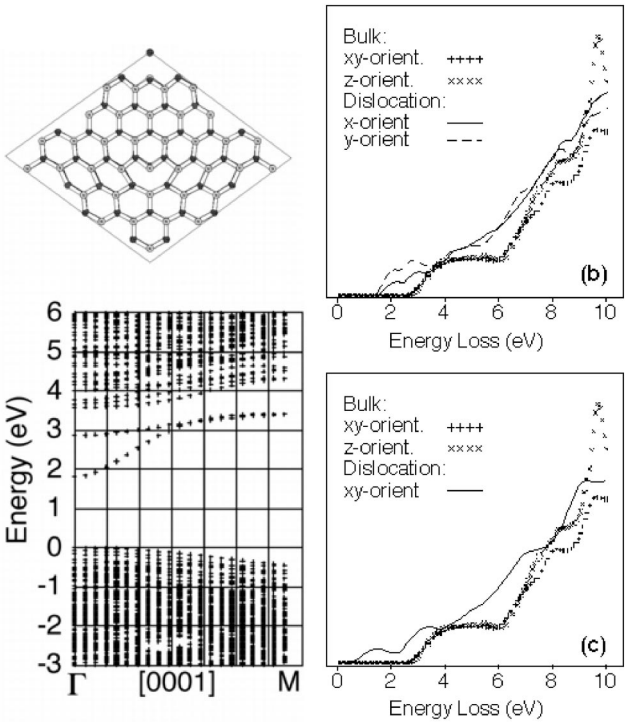

FIG. 4. (a) Atom positions and theoretical band structure of an edge dislocation in GaN, along the core of the dislocation in the [0001] direction. The reference energy has been set at the top of the filled valence states. All levels above the valence band maximum are empty in undoped material. (b) Theoretical EEL spectra for bulk and edge dislocation with electron beam direction along the *c* axis (*z* orientation) and perpendicular to the *c* axis (*x* and *y* orientations). (c) Same as (b) but for full core screw dislocation.

lead to a supplementary absorption below the bulk band edge if the low EELS is performed on the dislocation. In order to model low loss spectra the calculated dielectric function is broadened using a Lorentzian function. The procedure is described in greater detail in Ref. 24. Figure 4(b) represents theoretical EEL spectra of a neutral edge dislocation and the bulk. Figure 4(c) shows the modeled low loss spectra for the screw dislocation and the bulk.

IV. SPATIAL RESOLUTION IN lowEELS AND ELNES

The impact parameter for low-energy scattering events is much larger than that for core-excitation losses. Results presented in Ref. 25 concerning spatially resolved EELS showed that the best achievable spatial resolution in the 1–10-eV energy-loss regime is 10 nm, whereas in the 400-eV energy-loss regime it can be 1 nm.

In a geometry where the dislocations are perpendicular to the electron beam (as it is the case in our GaN cross sections), the contribution of the dislocation line to the probe intersection volume is very small compared to that of the surrounding matrix. Rough estimates based on a 100–200-nm specimen thickness (typical for electron transparency) give ratios between the dislocation core and the volume of the matrix of the order of 1:1000. A core loss event with a 1-nm impact parameter will stem from a volume ex-

tending not much beyond the dislocation core. So the core loss signal resulting from the probe intersecting the dislocation line in cross sectional geometry will be very small compared to that of the surrounding matrix. The impact parameter increases by a factor of 10 for low loss scattering, and therefore the increase of the signal-producing volume around the dislocation core can be 100-fold. So the fractional contribution of the dislocation can be expected to increase to 1:20 in low loss, or in very thin regions even to 1:10. For this reason, dislocation effects can be seen in cross sectional geometry using lowEELS, but not in core loss spectroscopy. In contrast, for a plan view geometry where the electron beam progresses along the dislocation line, the ratio of the dislocation core to surrounding matrix volume can be as large as 1:10. Core loss spectroscopy will therefore pick up dislocation-induced effects in plan view geometry.[26]

For QWs, the situation is converse: with a probe intersecting a 5-nm-wide parallel QW, the major part of the core loss signal will originate from the QW. Due to the larger signal-producing volume with the low loss impact parameter, a much smaller fraction of the low loss signal will originate from the QW. In a multiple QW stack with 5-nm wells separated by 5-nm barriers the volume producing the low loss signal of wells and barriers will overlap, regardless of whether the probe is placed on a well or a barrier. Owing to this effect and the small In concentrations, the bandgap values measured in several $(In_{0.15}Ga_{0.75})_{0.5}N_{0.5}$ wells can be seen to scatter around a value close to 3.4 eV, typical of pure GaN. The rather large scatter in the bandgap values is attributed to phase segregation in the InGaN alloy.[27] The volumes producing the core loss signals do not overlap, and here differences of the N edge in the QW's and the barriers could be detected [see peak ratios between *A*, *B* and *C* in Fig. 7(a)].

The same criteria apply for AlGaN QWs in a later paragraph. The Al-concentration in the wells is 15%, and the QW signature can be seen in ELNES [see Fig. 7(b)], but not in lowEELS, whereas dislocation effects are detectable in lowEELS, but not in ELNES.

V. RESULTS AND DISCUSSION

A. Interfaces

GaN/sapphire interface. In sample 1, the first 40 nm of the GaN constitute a buffer layer grown at low temperature. High-resolution transmission electron micrographs of this buffer region showed continuous faulting in the basal plane (results not shown here), producing a transformation of this region into cubic phase domains. We measured values of the band gap of around 3.2 eV in these regions [Fig. 5(c)], in agreement with previous data for cubic GaN (*c*-GaN).[4,28] Other papers in the literature also identified domains of *c*-GaN mixed with wurtzite GaN.[29,30] Figure 5(a) shows N *K*-edge spectra taken in the perfect material, in the buffer layer, and in the interface with the substrate. The buffer layer spectrum is consistent with that of *c*-GaN,[31] but is not uniformly found throughout the buffer layer. The N *K* edge of the interface is drastically different and resembles that of gas phase N_2 (Core-Loss Atlas, Gatan). Sequential spectrum acquisition in the same spot results in a gradual decrease of the highest peak, until the N-edge of GaN dominates. This might be due to molecular nitrogen being released near the interface by the electron beam as a result of sapphire nitridation or/and a phase transformation. In Fig. 5(b) the EDX profiles of O, Al, Ga, and N taken along the arrow in Fig. 5(c) show that the interface is not abrupt, which suggests there could be interdiffusion between species of the Al_2O_3 and the GaN. Similar irregularities measuring the conductivity of sapphire/GaN interfaces of hydride vapor phase epitaxy grown samples have been detected using several scanning probe techniques.[32]

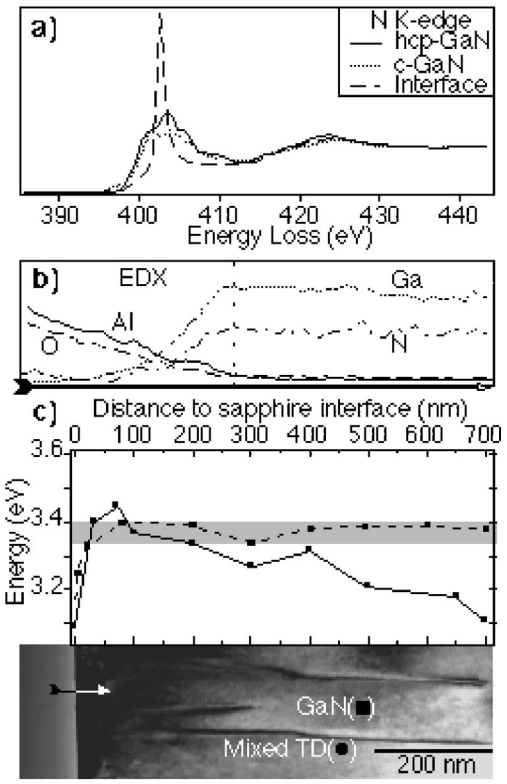

FIG. 5. (a) N *K*-edge ELNES taken in the wurzite GaN layer (solid line), in the GaN buffer layer (dotted line), and at the interface with the sapphire (dashed line). (b) EDX line scans taken along the arrow shown in (c). (c) EELS onset energies when stepping the electron beam along a dislocation line projection (circles) in an *n*-GaN film containing an InGaN/GaN QW structure at the film surface (not visible in figure) and parallel to the dislocation in the perfect material (squares). A STEM bright-field image of the dislocation, scaled to the size of the graph above, is also shown.

GaN/AlN/SiC. Figure 6(a) shows EELS onset energies obtained for an AlN/GaN structure with the electron beam stepped from the SiC buffer layer across a 20-nm AlN buffer into a GaN layer (sample 2). Al and Ga x-ray profiles show that SiC/AlN as well as the AlN/GaN interface are abrupt. The N *K*-edge ELNES obtained in the GaN and AlN layers are in agreement with published data for bulk GaN and AlN.[33,34] It is interesting to note that the N *K*-edge ELNES taken in the AlN within a few nm from the SiC interface (dash-dotted line spectrum) sometimes shows a similar strong gas phase N_2 peak as in the case of the ELNES of the

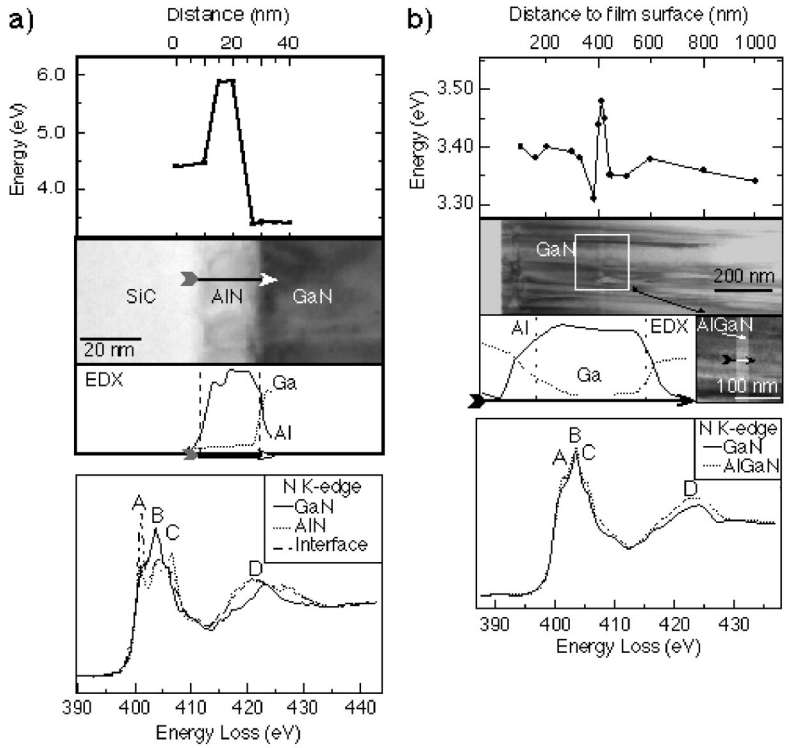

FIG. 6. (a) EELS onset energies (top panel) and x-ray line scans (in panel noted EDX) taken along the arrow shown in the bright field STEM image of an AlN/GaN structure grown on SiC. Also shown in the lower panel are N *K* edges of GaN (solid line), AlN (dotted line), and the interface between AlN and SiC (dash-dotted line). (b) EELS onset energies (top panel) and x-ray line scans (in panel noted EDX) measured across an AlGaN QW in GaN, together with bright-field STEM image and ELNES (lower panel) of the GaN (solid line) and the AlGaN well (dotted line).

GaN/sapphire interface. The peak decreases as the probe moves into the AlN layer. It reappears close to the AlN/GaN interface. Occasionally this peak is also seen in AlGaN/GaN QW interfaces. We currently have no explanation for the occurrence of this apparent excess nitrogen.

B. Quantum wells

AlGaN intralayer. Figure 6(b) shows EELS onset energies, together with a STEM image, x-ray profiles, and ELNES of a single 20-nm $(Al_{0.15}Ga_{0.85})_{0.5}N_{0.5}$ QW (sample 2). The first peak of the low loss derivative shows a distinctive trend when the electron beam is stepped across the QW, in that it shifts towards higher energies. At both edges of the QW the EELS onset energy seems to decrease. The variation of the EELS onset is not symmetrical with respect to the QW center, as is also found in the complementary set of x-ray line scans showing the Ga and Al profiles. Whereas the lower interface (on the right) is fairly abrupt in the x-ray line scan, the top interface (left) shows significant Ga-Al interdiffusion. The larger dip in the EELS onset energy at the top interface reflects the structurally inferior material quality. The low onset energies might be related to gap states due to accumulation of oxygen associated with the end of Al incorporation.

ELNES data of the N *K* edge of the single QW show a small increase in peaks *A* and *C* and a shift in peak *C* as well as an enhancement in the structure around peak *D*. These changes are in agreement with results measured in the transition from GaN to AlN (Refs. 34 and 35) and with our own measurements shown in Fig. 6(a). From calculations of the fundamental band gap of $Al_xGa_{1-x}N$,[33] the 3.5-eV gap seen in Fig. 6(b) corresponds to an Al fraction of ~10%. Since we have not adjusted the data to account for electron beam broadening in the sample, which leads to an underestimate of the concentration of thin layers embedded in a matrix of different stoichiometry,[36] this value is in reasonable agreement with the nominal value of Al of 15%.

InGaN and AlGaN QW's. Low EEL spectra have also been taken near the surface in the multiple quantum well region of the GaN structure of sample 1. The InGaN QW's are 5-nm thick and separated by 5-nm GaN barriers. Spectra are taken on consecutive QW's and barriers. As expected from the discussion in Sec. IV, low EELS of the InGaN QW's did not reveal differences in the EELS onset energies compared to the GaN barrier and to the GaN layer [Fig. 7(a), top]. There is, however, a considerable scatter in the energy values, which can be seen as resulting from stoichiometric and structural nonuniformity of the InGaN QW's.[27] The more localized ELNES data, in accordance with the discussion in Sec. IV, shows slight changes of the *A* and *C* peaks inside and outside the QW's [Fig. 7(a), bottom].

No change in the EELS onset energies could be detected when the electron beam is stepped across an AlGaN/GaN multiple QW array with 5-nm-wide $(Al_{0.15}Ga_{0.85})_{0.5}N_{0.5}$ QW's separated by 5-nm-GaN barriers [see Fig. 7(b), top]. The N *K* edge from a QW revealed changes in the relative peak heights *A*, *B*, and *C* [see Fig. 7(b), bottom], similar to the InGaN multiple-QW structure.

C. Dislocations

GaN with p-n doping. All bulk spectra of sample 3 show a featureless pre-bandgap region and a sharp rise at the band gap (3.4 eV), followed by a step and a plateau region starting at around 4 eV. This is demonstrated in Fig. 8(a) in curve *m*. It is worth noting that in undislocated, i.e., bulk material, this

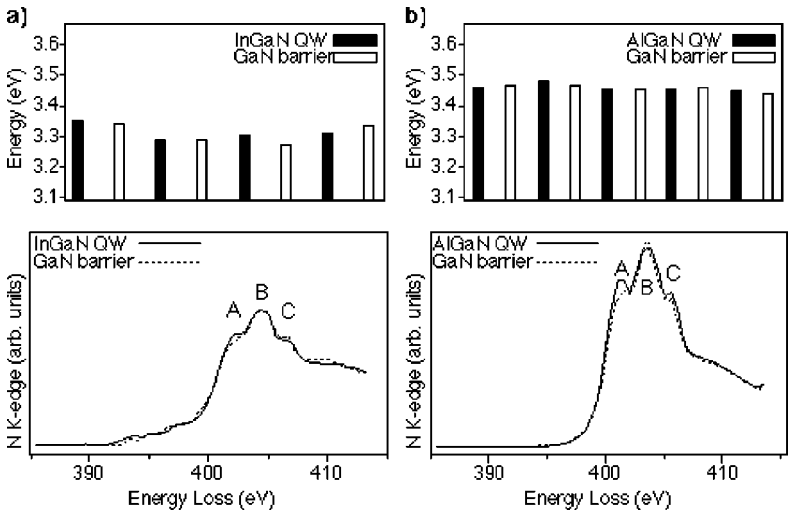

FIG. 7. (a) EELS onset energies of successive QW's and barriers (top panel) together with N *K*-ELNES of an InGaN MQW structure (lower panel). (b) Equivalent results for an AlGaN MQW structure.

plateau extends to about 6 eV, where it is followed by a further rise in the scattering intensity (see Fig. 3). ''Clean'' spectra like these indicate good quality bulk material. No change in the spectra can be seen as the beam crosses from *n*- to *p*-doped region. As the doping only induces a minor shift in the bandgap, this shift would be expected to lie within the accuracy error of the method. A major feature of dislocated material is the lack of a distinct plateau region; dislocations tend to introduce a more or less continuous rise in the scattering intensity above the band gap. This situation is depicted in the spectra in Fig. 8(a): *a* is a dislocation in the *n*-doped part and *b* and *c* are dislocations in the *p*-doped part; the spectra are similar for all dislocations investigated. As spectra like those shown in Fig. 8(a) contain signals from the dislocation core as well as the surrounding matrix, we shall call them compound spectra. The sample was rather thick at this point (approximately 200 nm), which is reflected in the high noise level of the spectra. Consequently the dislocation effects are very small, as expected from considerations in Sec. IV, and so in order to enhance the dislocation effects difference spectra were calculated. These were obtained by subtracting a bulk spectrum (i.e., spectrum *m*) of the vicinity from the dislocation spectrum in each case. In order to account for small differences in film thickness at the dislocation and the corresponding bulk spectrum position, the compound and bulk spectra intensities were normalized at around 9 eV prior to subtraction, since above this energy, according to the calculations, the dislocation effects become small. The difference spectra *a*-*m*, *b*-*m*, and *c*-*m* in Fig. 8(a) exhibit a pre-band-gap peak followed by a general rise in intensity. These features are significantly weaker in difference spectra taken of various bulk positions (curve Δm). The accuracy

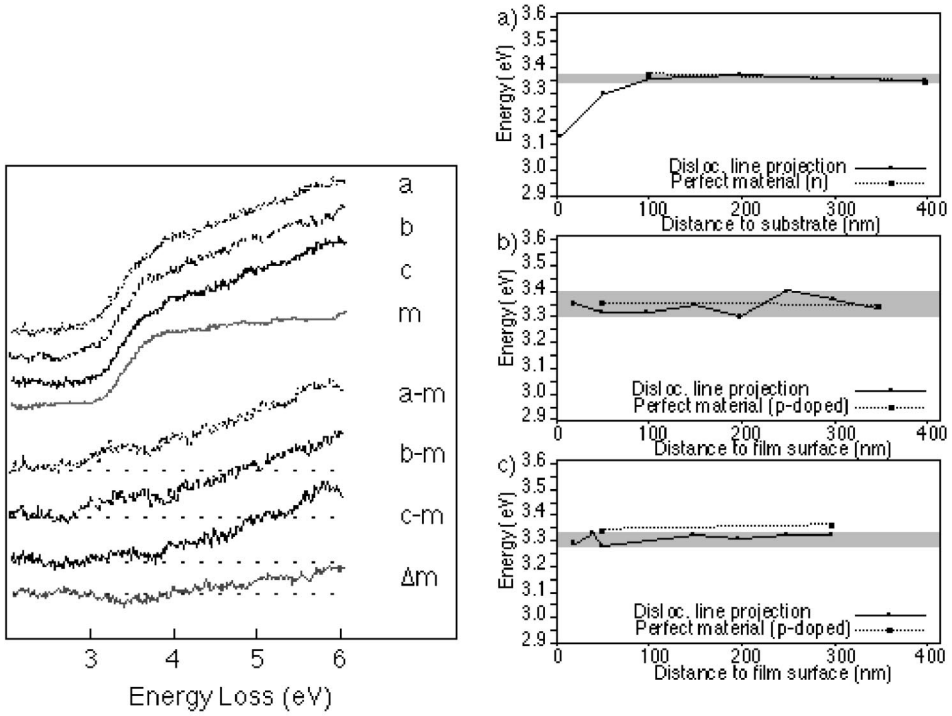

FIG. 8. (a) Low EEL compound spectra taken of a point on dislocation line projections in *n*-doped (curve *a*) and *p*-doped (curves *b* and *c*) GaN. Curve *m* is of bulk material. Curves *a*-*m*, *b*-*m*, *c*-*m*, and Δm are the difference spectra of the respective compound spectrum above and the bulk spectrum. (b) Top panel: onset energies measured along a mixed threading dislocation projection in *n* material (solid line), together with the values of the perfect material (dashed line) (sample 2). Middle and bottom panels: same as top panel for a mixed and a screw dislocation, respectively, in *p*-type material (sample 3).

limit of the measurement produces slight energy shifts between different spectra, therefore a small peak (or dip) at the band gap will always be present in difference spectra even if spectra are taken in identical locations. The plateau region also varies slightly from bulk spectrum to bulk spectrum (we believe this is a specimen thickness-induced effect), hence the very slow rise in curve Δm. These differences are, however, consistently larger in dislocated regions; the peak at around 3.3 eV can even just about be seen in the compound spectra as extended tail in the intensity rise at the band gap, whereas the general continuous rise above 4 eV can readily be seen in the compound spectra. The difference spectra of the dislocations are in qualitative agreement with the calculated spectra in Figs. 4(b) and 4(c). They bear greatest similarity with the spectrum in Fig. 4(c) of a full core neutral screw dislocation, which exhibits pre-band edge peak at around 3.3 eV. Our dislocations are of mixed and screw characters; hence the effect of the screw component ought to be present in all cases. According to the calculations transitions into deep levels should also occur at 1.5 eV, but, as mentioned in Sec. II, we cannot presently extract features below 2 eV with great reliability. It is also worth noting that no difference can be seen between dislocation spectra in the *p* and *n* regions. Without demonstration we want to note that calculations of negatively charged edge dislocation spectra (i.e., of *p*-doped material) (Ref. 37) reveal marked differences in the pre-band-edge region (the pre-edge peak shifts down to 1 eV and the band edge itself is smeared out down to 2 eV). As we do not see this behavior we conclude that the doping is inactive.

The top panel of Fig. 8(b) plots the EELS onset energies as a function of position, as the beam is stepped along a dislocation line projection in the *n*-type material from sample 2. The first derivative of the spectrum is calculated for each beam position, with the band-gap-related onset energy defined by the position of the lowest energy peak. The EELS onset energies associated with the dislocation assume a value of 3.13 eV near the interface with the SiC substrate. This value of the onset energy corresponds to the presence of the cubic nitride phase (as described in Sec. V A). We also find that the onset energy rises to an asymptotic value of 3.31 eV (associated with hexagonal bulk GaN) as the beam moves away from the interface. The onset energies associated with the dislocations are found to be within 0.02 eV of the values for the perfect material. The statistical errors inherent in the measurement of the onset energies are indicated by the gray bands shown in Fig. 8(b). The middle and bottom panels of Fig. 8(b) map the onset energies as a function of beam position for sample 3. Here the onset energies for screw and mixed dislocations within the *p*-type region are plotted as a function of distance from the p/n interface. The bulk results fall within the scatter band of the EELS onset energies for the screw dislocation, whereas the onset energies for mixed dislocation fall just outside the bulk scatter band. These results indicate that the contribution of dislocations to the onset energy is relatively small. Indeed, the presence of dislocations seems only to add to the intensity of the pre-band-edge region, as shown in Fig. 8(a).

One might ask how the statistical error can be so small in view of the energy resolution of the method (± 0.18 eV). The energy resolution of the instrument, described by the energy range outside which two spectral features may lie so as to be recognized as separate features, must not be confused with the accuracy, with which a singular feature can be positioned. Since all spectra are aligned to each other with respect to the position of their ZLPs, this accuracy is neither dependent on the spread of the field emission function nor on the high voltage stability (both of which contribute to the FWHM of the ZLP, which in turn defines the energy resolution). It is predominantly dependent on the spectrometer characteristics, e.g., the channel width stability, and this introduces a far smaller error than the FWHM of the ZLP. This error is difficult to estimate, but we can see its manifestation in the statistical error of the measurement.

GaN with QWs. An EEL spot analysis was also carried out at a number of locations along dislocations in sample 1. The beam was stepped along the dislocation line projection and the spectra compared to those obtained when the beam was stepped in similar intervals in the perfect material parallel to the dislocation. Spectra taken with the probe stepped along several mixed dislocations showed a continuous decrease in the EELS onset energy from the Al_2O_3 interface toward the GaN surface. An example is shown in Fig. 5(c) where EELS onset energies are displayed for material containing the dislocation and for perfect material as a function of the distance from the Al_2O_3 interface. In both graphs in Fig. 5(c) there is a $\sim$40-nm region where the value of the EELS onset energy is smaller than the gap of hexagonal GaN which we ascribe to cubic phase inclusions (see Sec. V A). Decoration of the dislocation with Al could explain that the EELS onset energies beyond the buffer, between 40 and 100 nm from the interface, also shown in Fig. 5(c), seem to be higher than values normally expected for GaN.

As the beam is stepped along the projected core of the threading dislocation towards the GaN film surface, a decrease in the EELS onset energies [Fig. 5(c)] from 3.4 eV (the band gap of *w*-GaN) to 3.1 eV is found. Considering the accuracy of the energy measurement as explained above we argue that the difference in the EELS onset energies between the bottom and the top of the thin film, as well as in the buffer, is significant.

The shift in the EELS onset along the dislocation line could be due to a migration of point defects, such as vacancies or O from the surface, or In migration from the QW region down the dislocation core. Several studies have indeed led to the conclusion that threading dislocations in particular could enhance pipe diffusion of impurities and vacancies.[2] Indium diffusion from the GaN film surface finds strong support from our own studies.[27] Using x-ray line scans taken across dislocations threading through InGaN QW's, we have previously measured In accumulation within, and a depletion of In surrounding, dislocations. The fact that this phenomenon could be measured by x-ray techniques suggests that the localized In inhomogeneities are quite high. One would thus expect it to be noticeable in low EELS too, as the gap of GaN is lowered when indium is added. Another possible explanation for the reduction in the EELS onset

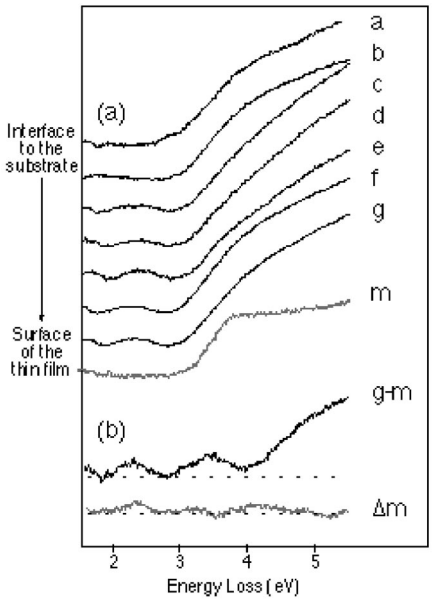

FIG. 9. (a) Low EEL spectra taken along a mixed threading dislocation [Fig. 5(c)] in an undoped (*n*-type) GaN cross sectional film, with an InGaN MQW near the GaN film surface. (b) Difference spectrum of the dislocation at a position approximately three-fourths of the film thickness away from the substrate; the bottom curve is the difference of two bulk spectra.

energy toward the sample surface could be found in a decrease in the TEM-sample thickness. The dislocation effects would become stronger as the ratio of the dislocation volume to the surrounding matrix increased (i.e., in thinner regions). Since the energy resolution is ± 0.18 eV, scattering into levels lying within this energy range below the band gap, given their proportion in the electron beam interaction volume is high enough, would become noticeable as a shift in the EELS onset energy. The thickness of the sample in Fig. 9 indeed decreased toward the surface. It should be noted that the sample of Fig. 8 was thicker throughout than the sample in Fig. 9.

Figure 9(a) shows compound spectra $a-g$ of the low loss region taken at various points along the dislocation line from the interface in direction towards the surface. As noted before the dislocation spectra show a much more continuous rise than the bulk spectrum *m*. Attention is drawn to a feature at 2.4 eV, which emerges half way along the dislocation line toward the sample surface. It can also be seen in spectra taken up to a few tens of nm away from the dislocation line near positions *f* and *g*, which are positioned roughly at about three-fourths of the film thickness toward the surface. The feature is not present in all the GaN materials under our investigation, e.g., it was not detected in the sample of Fig. 8, and it is not reproduced in the spectrum calculations. It is likely that this transition is not arising due to a property of the dislocation, but to point defects, which have accumulated in the strain field of the dislocation.[12] It corresponds energetically to the transition energy for yellow luminescence.

Figure 9(b) shows a difference spectrum $(g-m)$. The spectrum has the same shape as these in Fig. 8(a) and again is in closest qualitative agreement with the calculated spectrum for the neutral screw dislocation in Fig. 4(c). The spectrum statistics is improved because the sample is overall thinner, and the peak at 3.3 eV is more pronounced than in Fig. 8(a). Its contribution is so strong here that it might well be responsible for the band-gap shift seen in Fig. 5(c). The bulk difference spectrum Δm shows a much weaker pre-band-edge feature (peak or dip depending on which way the difference is taken) and a much shallower gradient between 4 and 6 eV. The peak at 2.4 eV bears witness of the fact that some bulk spectra, especially near dislocations, exhibit a transition at this energy.

The results presented here are to our knowledge the first measurements to show evidence, via low EELS, of dislocation-induced effects on the local crystal band structure. The observations are strongly backed up by model calculations. The effects of dislocation cores on the ELNES of the N *K* edge, when measured in cross-sectional geometry, are much less pronounced than on the low EELS and therefore more debatable.

VI. CONCLUSIONS

Highly localized EELS in the energy-loss regime at band gap of cross-sectional GaN InGaN, and Al(Ga)N structures, complemented by N *K*-edge ELNES measurements and x-ray line scans, have been presented. We have determined the band-gap-related EELS onset energies of heterointerfaces, of QW's and of dislocations, using a very high EEL spectrometer dispersion. The energy resolution and error regime of the system have been discussed, highlighting the fact that the accuracy of positioning features in the low loss spectrum is significantly smaller than energy resolution, thereby allowing our measurements to yield meaningful results.

Calculated low loss spectra of GaN and AlN were found to be in very good agreement with experimental spectra, reproducing the correct spectral shape of band-to-band transitions within the energy resolution of the experimental technique. The EELS onset energies of a single AlN and AlGaN QW have been obtained, as well as the characteristic ELNES spectra. In MQW structures of InGaN and AlGaN the corresponding EELS onset energies of individual wells and barriers cannot be discerned, whereas ELNES of the wells and barriers exhibits the fingerprint of the respective material. This is thought to be due to the relatively weaker localization of the initial state in low loss spectroscopy compared to core loss scattering. The low loss signals of multiple wells and barriers therefore overlap, and are thus averaged out.

Low loss spectra obtained on spatially isolated dislocation line projections showed modifications over the bulk spectra, whereas no changes were detected in the ELNES. It is thought that in contrast to the low energy scattering regime the high localization of the core loss signal is of disadvantage here as it is drowned by the signal of the matrix, which is simultaneously excited by the electron probe.

Difference spectra of the low loss regime of threading dislocations in GaN films showed a pre-band-edge feature and a continuous rise in the signal above the band edge. This was found to be in agreement with low EEL spectrum calcu-

lations based on energy states of dislocations in GaN obtained from self-consistent *ab initio* simulations within the LDA to density-functional theory. Best agreement is obtained with the calculated full core neutral screw dislocation spectrum.

In some cases a decrease in the EELS onset energy was measured as the probe was stepped along a dislocation projection toward the film surface. One possible explanation was In diffusion from an InGaN MQW structure grown near the film surface along the dislocation core. But it was thought more likely that the high contribution of the preband-edge levels at the dislocation core induce this shift in thin samples; due to the low-energy resolution of the technique, transitions involving these levels are not resolved as separate peaks in the compound spectra. A peak at 2.4 eV is observed in the vicinity of dislocations in some GaN materials. This is not shown in the calculations, and is therefore thought to be due to impurity or point defect accumulation in the dislocation strain field.

ACKNOWLEDGMENTS

We would like to thank K. Jacobs and I. Moerman of the IMEC, Gent for supplying the *n-p* GaN and GaN/InGaN materials, and A. Rizzi of the Forschungszentrum Juelich for supplying the GaN/AlGaN material. We also thank Jiang-Guo Zheng for his assistance with the STEM measurements and N. Duxbury, C. Dieker, and H. Darwish for TEM sample preparation. The work was carried out under EPSRC Grant No. GR/M29719.

[1] J. S. Speck and S. J. Rosner, Physica B **273–274**, 24 (1999).
[2] M. Haugk, J. Elsner, T. Frauenheim, T. E. M. Staab, C. D. Latham, R. Jones, H. S. Leipner, T. Heine, G. Seifert, and M. Sternberg, Phys. Status Solidi B **217**, 473 (2000).
[3] G. Brockt and H. Lakner, Mater. Sci. Eng., B **59**, 155 (1999).
[4] D. Chandrasekhar, D. J. Smith, S. Strite, M. E. Lin, and H. Morkoc, J. Cryst. Growth **152**, 135 (1995).
[5] N. Duxbury, U. Bangert, P. Dawson, E. J. Thrush, W. Van der Stricht, K. Jacobs, and I. Moerman, Appl. Phys. Lett. **76**, 1600 (2000).
[6] J. E. Northrup, L. T. Romano, and J. Neugebauer, Appl. Phys. Lett. **74**, 2319 (1999).
[7] S. J. Rosner, E. C. Carr, M. G. Ludowise, G. Girolami, and H. I. Erikson, Appl. Phys. Lett. **70**, 420 (1997).
[8] F. A. Ponce, D. P. Bour, W. Gotz, and P. J. Wright, Appl. Phys. Lett. **86**, 57 (1996).
[9] P. E. Batson, K. L. Kavanagh, J. M. Woodall, and J. W. Mayer, Phys. Rev. Lett. **57**, 2729 (1986).
[10] Y. Xin, E. M. James, I. Arslan, S. Sivananthan, N. D. Browning, S. J. Pennycook, F. Omnes, B. Beaumont, J. P. Faurie, and P. Gibart, Appl. Phys. Lett. **76**, 466 (2000).
[11] A. Nagayama, H. Sawada, E. Takuma, R. Katayama, J. Wu, K. Onabe, H. Ichinose, and Y. Shiraki, Phys. Status Solidi B (to be published).
[12] J. Elsner, R. Jones, P. K. Sitch, V. D. Porezag, M. Elstner, Th. Frauenheim, M. I. Heggie, S. Oberg, and P. R. Briddon, Phys. Rev. Lett. **79**, 3672 (1997).
[13] A. F. Wright and U. Grossner, Appl. Phys. Lett. **73**, 2751 (1998).
[14] J. E. Northrup, Appl. Phys. Lett. **78**, 2288 (2001).
[15] K. Jacobs, W. Van Der Stricht, I. Moerman, P. Demeester, J. De Naeyer, S. Verstuyft, P. Van-Daele, D. M. Tricker, A. Amokrane, S. Dassonnneville, B. Sieber, and E. J. Thrush, Paper presented at European Workshop MOVPE (EW-MOVPE VIII), Prague, June 1999.
[16] A. Rizzi, R. Lantier, F. Monti, H. Luth, F. Della Sala, A. Di Carlo, and P. Lugli, J. Vac. Sci. Technol. B **17**, 1674 (1999).
[17] D. Lancefield (private communication).
[18] B. Rafferty and L. M. Brown, Phys. Rev. B **58**, 10 326 (1998).
[19] T. Grenet and M. C. Cheynet, Eur. Phys. J. B **13**, 701 (2000).
[20] P. R. Briddon and R. Jones, Phys. Status Solidi B **217**, 131 (2000).
[21] G. B. Bachelet, D. R. Hamann, and M. Schlüter, Phys. Rev. B **26**, 4199 (1982).
[22] D. Nozières and D. Pines, Phys. Rev. **113**, 1254 (1959).
[23] G. F. Bassani, and G. Pastori-Parravicini, in *Electronic states and Optical Transitions in Solids*, edited by R. A. Ballinger, International Series of Monographs in the Science of the Solid State Vol. 8 (Pergamon, Oxford, 1975).
[24] C. J. Fall, A. T. Blumenau, R. Jones, P. R. Briddon, A. Gutiérrez-Sosa, U. Bangert, A. E. Mora, T. Frauenheim, J. W. Steeds and J. E. Butler (unpublished).
[25] M. K. H. Natusch, G. A. Botton, and C. J. Humphreys, Inst. Phys. Conf. Ser. **157**, 213 (1997).
[26] A. Gutiérrez-Sosa, U. Bangert, and A. J. Harvey (unpublished).
[27] N. Duxbury, U. Bangert, P. Shang, E. J. Thrush, and K. Jacobs, Inst. Phys. Conf. Ser. **161**, 207 (1999).
[28] C. Noguez, Phys. Status Solidi A **175**, 57 (1999).
[29] X. H. Wu, P. Fini, E. J. Tarsa, B. Heying, S. Keller, U. K. Mishra, S. P. DenBaars, and J. S. Speck, J. Cryst. Growth **189/190**, 231 (1998).
[30] M. Katsikini, E. C. Paloura, and T. D. Moustakas, J. Appl. Phys. **83**, 1437 (1998).
[31] S. Oktyabrsky, K. Dovidenko, A. K. Sharma, J. Narayan, and V. Joshkin, Appl. Phys. Lett. **74**, 2465 (1999).
[32] J. W. P. Hsu, D. V. Lang, S. Richter, R. N. Kleiman, A. M. Sergent, and R. J. Molnar, Appl. Phys. Lett. **77**, 2873 (2000).
[33] T. Wethkamp, K. Wilmers, N. Esser, W. Richter, O. Ambacher, H. Angerer, G. Jungk, R. L. Johnson, and M. Cardona, Thin Solid Films **313–314**, 745 (1998).
[34] M. Katsikini, E. C. Paloura, M. Fieber-Erdmam, E. Holub-Krappe, D. Korakakis, and T. D. Moustakas, J. Electron Spectrosc. Relat. Phenom. **103**, 695 (1999).
[35] L. C. Duda, C. B. Stagarescu, J. Downes, K. E. Smith, D. Korakakis, T. D. Moustakas, J. H. Guo, and J. Nordgren, Phys. Rev. B **58**, 1928 (1998).
[36] U. Bangert, A. J. Harvey, C. Dieker, A. Hartmann, and R. Keyse, Philos. Mag. A **74**, 1421 (1996).
[37] C. J. Fall, R. Jones, P. R. Briddon, M. I. Heggie, A. Gutiérrez-Sosa, and U Bangert (unpublished).